On the Design of NMR Sensor for Well-Logging Applications

Jaideva C. Goswami, *Senior Member, IEEE,* Apo Sezginer, *Senior Member, IEEE,* and Bruno Luong

***Abstract*—The magnetic fields of antenna and magnet used in inside-out nuclear magnetic resonance (NMR) well-logging tool are computed using a finite-element method (FEM). A typical operating frequency of such tools is 2 MHz, at which the skin depth is about 47 μm for copper conductor. A direct application of FEM to evaluate power loss at such frequency, therefore, requires very fine discretization of the conductors, which, in turn, makes the problem numerically ill-conditioned. A perturbation technique along with FEM is used to evaluate the power loss in conductors that avoids the need for small discretization steps along the conductor thickness. The design of the magnet, on the other hand, is complicated by the fact that the model is nonlinear in nature because of the presence of ferrites and steel materials surrounding the magnet and because the size of the problem is usually quite large; quarter of a million unknowns is fairly common. A typical nonlinear FEM model requires about 35 h of central processing unit (CPU) time on a Sun Ultra 60 296 MHz workstation with one gigabyte of RAM. The magnet is built by stacking several magnet segments along the axial direction and the objective of the design is to magnetize these segments in such a way so as to produce a desired field profile in front of the magnet. It generally requires many executions of the nonlinear FEM model. An optimal control technique is used in conjunction with the FEM to speed up the design process. Very good agreement between the measured and computed antenna efficiency and magnetic field is obtained thus validating the numerical model.**

***Index Terms*—Antenna, finite-element method (FEM), magnet, nuclear magnetic resonance, oil exploration, well logging.**

I. Introduction

NUCLEAR magnetic resonance (NMR) techniques have been in use for many years in chemistry and biochemistry laboratories to analyze the molecular structure of compounds. In this technique, a sample is placed inside a coil that produces a time varying magnetic field in the presence of a static magnetic field generated by an external magnet. The measurement of spin–lattice relaxation time (T_1), spin–spin relaxation time (T_2), frequency spectrum, and coupling between resonances then provide valuable information about the molecular composition of the sample.

In the last few years, NMR measurements have become an important part of oilfield well logging to identify and quantify oil and gas reservoirs. For such applications, the major problem comes from the fact that the sample (earth formation) is outside the sensor, as shown in Fig. 1. Furthermore, at a depth of about 5 km, a typical well depth, the NMR instrument has to withstand hostile conditions such as high temperatures (175°C), high pressures (20 000 psi), corrosive fluid, low power, and high mechanical shocks. In addition, the instrument must be designed to fit inside a small hole (typically 6–12 in in diameter). The Johnson noise generated by the conductors and magnetoacoustic ringing caused by RF current-carrying conductors in the presence of static magnetic field significantly affect the quality of the received signal. There are thus many challenges in designing an oil-field NMR instrument, including the design and selection of electronics that can operate the instrument, process the NMR information, and work under hostile conditions typical of oil wells.

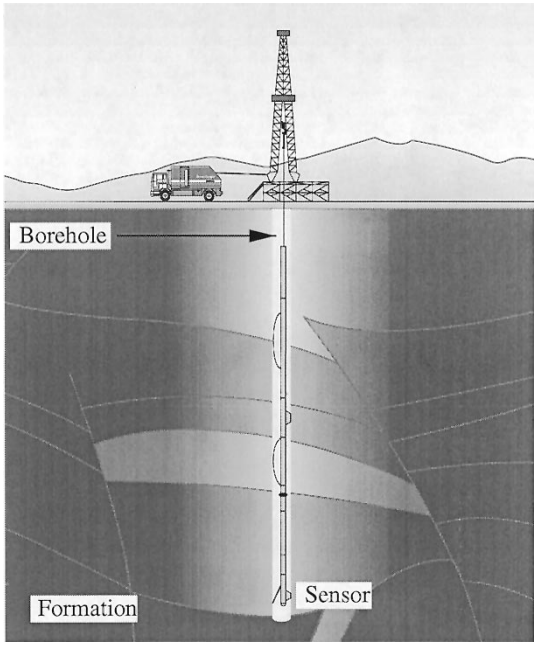

Fig. 1. A well-logging tool inside a borehole.

Several inside-out NMR instruments have been proposed [1]–[8]. In this paper, we concentrate on the instrument configuration of [8] and discuss efficient numerical techniques for the analysis and design of magnets and antennas for such configuration. The cross section of this configuration is shown in Fig. 2. The antenna is sandwiched between two permanent magnets. It is worth mentioning here that antenna in NMR well-logging tool is a near-field antenna and not a far-field one, commonly employed in microwave communications. These antennas are generally designed to see through a few inches in the formation. Computation of power loss in the antenna is very important in evaluating the performance of a particular design. Method of moments has been used to evaluate the efficiency of such an antenna [9]. Because of the complexity of the geometry

Manuscript received August 26, 1999; revised March 17, 2000.

The authors are with Sugar Land Product Center, Schlumberger Oilfield Services, Sugar Land, TX 77478 USA (e-mail: jcgoswami@ieee.org; aposezginer@slb.com; bluong2@slb.com).

Publisher Item Identifier S 0018-926X(00)09361-3.

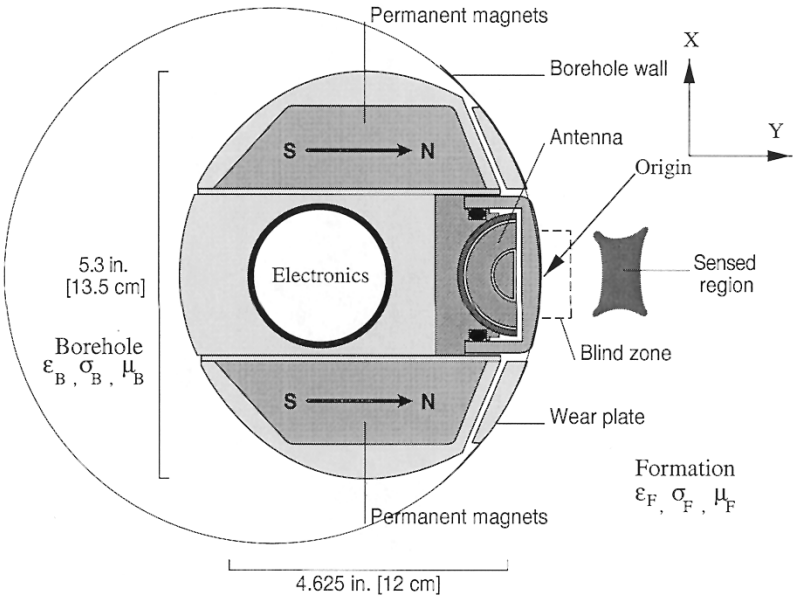

Fig. 2. Cross section of an inside-out NMR well-logging sensor. The sensor is pressed against the borehole wall by spring actions.

and materials, finite-element method (FEM) is found to be quite useful. However, a direct application of FEM to compute power loss in a conductor proves to be inefficient since the skin depth at about 2 MHz, a typical operating frequency for such tool, is quite small. A perturbation technique is used to evaluate the power loss, which requires the knowledge of tangential components of the magnetic field only at the surface of the conductors. As a result, we can get accurate values for the power loss even by coarsely discretizing the antenna conductors.

The magnets shown in Fig. 2 are magnetized so as to get a saddle point in the formation. The magnet is built by stacking several magnet segments along the axial direction. Such an arrangement is shown schematically in Fig. 3. The objective is to magnetize each segment in such a way so as to produce a desired field profile in front of the sensor. Efforts are made so that each magnet piece is fully saturated at the time of magnetization. While achieving a particular magnetization direction is easy (simply orient the material in the desired direction at the time of magnetization), the desired magnitude is achieved by adjusting the volume of the magnet material.

In the tool, the magnet is surrounded with nonlinear magnetic materials such as ferrites, steel, etc., which are primarily used in the antenna or in shielding the electronic components from strong magnetic field. As mentioned before, it takes about 35 h of central processing unit (CPU) time on a Sun Ultra 60 296 MHz workstation, with 1 GB of RAM and a complete design cycle takes many executions of nonlinear model. An optimization technique in conjunction with FEM is used to speed up the design process.

The rest of the paper is organized as follows. Some basic NMR principles are discussed in Section II along with the analysis and design of antenna and magnet. Numerical and experimental results are presented in Section III. Finally, in Section IV, we summarize the findings of this paper.

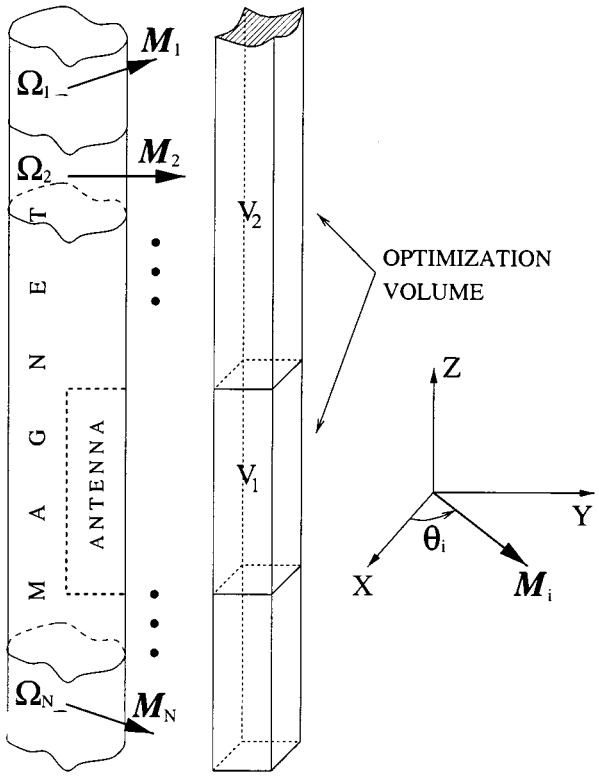

Fig. 3. Geometry of the magnet segments and the volume in which the field profile is optimized.

II. Theory

From an NMR petrophysical perspective, earth formation is a collection of hydrogen nuclei with randomly distributed dipole moments. In the presence of an external static magnetic field $(\mathbf{B_0})$, these nuclei tend to align with and precess around the

direction of the applied field. As will be discussed in the following section, an RF pulse is required to activate these nuclei and make them emit energy, which then can be received by a properly tuned antenna. Hydrogen nucleus or a proton has two spin states: spin up and spin down, both with almost equal probability. These probabilities based on Maxwell–Boltzmann distribution are 0.500 001 70 for spin up and 0.499 998 30 for spin down at room temperature and 500 Gauss of $|\mathbf{B_0}|$. Consequently, strength of the received signal is very weak (signals from spin-up and spin-down nuclei cancel each other)—of the order of a few hundred nV, which, given the hostile well-logging environment, is comparable to the Johnson noise (100 Ω resistor at 175 °C produces about 250 nV of noise signal for 25 kHz bandwidth), noise in the electronics, and magneto-acoustic ringing.

The signal voltage v induced at the terminals of the RF antenna due to a point-magnetic dipole $\mathbf{m}$ at the location $\mathbf{r}$ can be computed by using the reciprocity theorem that gives

$$v = j\omega \frac{\mathbf{B_1}(\mathbf{r}, \omega)}{I} \cdot \mathbf{m} \tag{1}$$

where $\mathbf{B_1}$ is the RF field produced by the antenna at the location $\mathbf{r}$ of the dipole and I is current at the terminal of the antenna. The total signal received by the antenna can be computed by evaluating a volume integral of (1) over the formation region and by taking into account the transfer function of the receiver and the spin dynamics. Significant contributions to the space integral come from a region that is close to or on resonance, given as

$$|\gamma|\mathbf{B_0}| - \omega| \lesssim \gamma|\mathbf{B_1^{\perp}}| \tag{2}$$

where

- γ gyromagnetic ratio, to be discussed shortly;
- ω RF frequency;
- $\mathbf{B_1^{\perp}}$ component of $\mathbf{B_1}$ orthogonal to $\mathbf{B_0}$.

Our objective is to design the tool to maximize the signal-to-noise ratio (SNR). Computation of SNR is mathematically quite involved and is not necessary to understand this paper. Interested readers may refer to [8], [9] for details. But for the present discussion, it is sufficient to consider (1) and (2) and observe that we can increase the NMR signal by increasing the resonant volume from where the dipoles will contribute to the overall signal and this we can do by producing uniform static magnetic field over as wide a region as possible [thereby reducing the left-hand side of (2)] and by increasing the RF field [thereby increasing the right-hand side of (2)]. The homogeneity of static magnetic field is also an important consideration to account for the tool motion during the acquisition period (usually a few seconds) of NMR signal. The strength of the RF field is limited by the availability of power. In this paper, we will compute the power loss in the antenna, which is basically a one-turn coil with ferrite, arranged in such a way that it produces RF field that is orthogonal to the static field in the region of interest. Magnet design, on the other hand, provides a lot of opportunity for optimization of the tool design since we use a permanent magnet and once it is built, it does not depend on the limitations of the electronic circuitry.

In this section, we discuss numerical methods for the analysis and design of antenna and magnet shown in Fig. 2. Before we proceed any further, it is worthwhile to go through some of the basics of NMR and their relation to oilfield exploration. Further details on NMR may be found in [10]–[12].

A. NMR Fundamentals

As mentioned in the previous section, in NMR technique (pulsed NMR, for our applications), a sample is placed in a static magnetic field so that all the magnetic dipoles get aligned with the external magnetic field. An RF pulse is applied. The combination of the RF and static magnetic field causes magnetic dipoles to tip from their equilibrium orientation and precess about the direction of the resultant field with a frequency $\omega_{\mathbf{0}}$, known as the Larmor frequency. When the RF field is removed, the magnetic dipole moments return to their original orientation. The time constant with which the axial (along $\mathbf{B_0}$) components of these moments return to the equilibrium orientation is called spin–lattice relaxation time (T_1), while the time constant with which the transverse components reduce to zero is called spin–spin relaxation time (T_2). Measurement of these two time constants renders many important properties of the sample.

The magnetic dipole moment $(\mathcal{M})$ of a nucleus is related to its spin angular momentum $(\mathbf{S})$ as $\mathcal{M} = \gamma\mathbf{S}$ where γ is the gyromagnetic ratio ($\gamma/2\pi = 4.258$ kHz/Gauss for protons). The rate of change of angular momentum is the torque $\mathbf{T}$ experienced by the dipole and is related to the external field $\mathbf{B_0}$ as

$$\mathbf{T} = \frac{d\mathbf{S}}{dt} = \mathcal{M} \times \mathbf{B_0}. \tag{3}$$

Thus

$$\frac{d\mathcal{M}}{dt} = \gamma\mathcal{M} \times \mathbf{B_0}. \tag{4}$$

Equation (4) is referred to as Bloch equation. Solution of this equation is precession of $\mathcal{M}$ about $\mathbf{B_0}$ with frequency $\omega_0 = -\gamma|\mathbf{B_0}|$. The precessing nuclei are in a state of equilibrium and no energy is emitted in such a state. A circularly polarized RF field $\mathbf{B_1}$ is required to activate the nuclei and make them emit energy. An RF pulse tips the precession axis of the nuclei by an angle $\theta = \gamma|\mathbf{B_1^{\perp}}|t_p$ where t_p is the width of the RF pulse (assumed here to be of square shape) and $\mathbf{B_1^{\perp}}$ is a component of $\mathbf{B_1}$ perpendicular to $\mathbf{B_0}$.

As noted before, when the RF field is removed the nuclei undergo a relaxation process in which energy is dissipated from the collection of nuclei, the "spin systems" to their atomic and molecular environment, the "lattice." The time constant associated with this relaxation mechanism is the spin–lattice relaxation time T_1. The spin–spin relaxation time T_2, on the other hand, is associated with the transverse relaxation process caused by mutual coupling between neighboring nuclei. When we include these many body interactions into (4), the Bloch equation modifies to

$$\frac{d\mathcal{M}}{dt} = \gamma\mathcal{M} \times (\mathbf{B_0} + \mathbf{B_1}) - \frac{\mathcal{M}_x\hat{\mathbf{x}} + \mathcal{M}_y\hat{\mathbf{y}}}{T_2} - \frac{(\mathcal{M}_z - \mathcal{M}_0)\hat{\mathbf{z}}}{T_1} \tag{5}$$

and the solution when RF pulse is removed and the static field is along $\hat{\mathbf{z}}$ becomes

$$\begin{cases} \mathcal{M}_x(\mathbf{r},t) = e^{-t/T_2}\left(\mathcal{M}_x^0(\mathbf{r})\cos\omega_0 t - \mathcal{M}_y^0(\mathbf{r})\sin\omega_0 t\right) \\ \mathcal{M}_y(\mathbf{r},t) = e^{-t/T_2}\left(\mathcal{M}_x^0(\mathbf{r})\sin\omega_0 t + \mathcal{M}_y^0(\mathbf{r})\cos\omega_0 t\right) \\ \mathcal{M}_z(\mathbf{r},t) = \mathcal{M}_z^0(\mathbf{r})e^{-t/T_1} + \mathcal{M}_0(\mathbf{r})(1-e^{-t/T_1}) \end{cases} \tag{6}$$

where $\mathcal{M}_0$ is the magnetization at the equilibrium state and $\mathcal{M}_x^0, \mathcal{M}_y^0$, and $\mathcal{M}_z^0$ are the components of the initial magnetization. In NMR well-logging the relaxation time constants are measured and correlated with the parameters of interests [13].

In oilfield exploration, our primary objective is to identify and quantify hydrocarbons and determine their commercial producibility. We apply a sequence of RF pulses known as CPMG (Carr–Purcell–Meiboom–Gill) [14], [15] in which a $\pi/2$-pulse (tipping the spins) is followed by a number of π-pulses (refocusing the spins) and the signal (echo) is acquired between two consecutive π-pulses. Fig. 4 shows the spin mechanism of dipole moments and the relation of the time constant T_2 to the pore size of the reservoir rocks. The relaxation phenomenon is more pronounced when the probability of energy exchange between the spins and other atoms is higher. In smaller pores, spins are in contact with the pore-boundaries more often than in larger pores. Consequently, T_2 in smaller pores is shorter and the signal decays faster. Likewise, heavier oil relaxes faster than lighter oil for the same pore size. It gives an indication, therefore, that by measuring the time constants, we can determine the pore size as well as the viscosity of the residing fluid. Observe that in practice a rock sample consists of pores with numerous sizes and that these pores may contain mixture of several fluids. As a result, a single exponential function does not fit the decaying signal curve; rather there is a distribution of relaxation time constants from which properties of reservoir rocks and fluids are extracted.

B. Antenna Analysis and Design

The antenna shown in Fig. 2 can be considered as a coaxial line, sliced axially. It can also be viewed as a one-turn coil. The region between the conductors of the antenna is filled with ferrites to increase its efficiency. Because of the nonuniform static magnetic field in the ferrite region, different parts of the ferrite saturates differently, thus resulting in an inhomogeneous permeability. The borehole is filled with special fluid to balance the pressure below the surface. These fluids may be conductive.

The main part of antenna analysis concerns the calculation of antenna efficiency (ε_A), defined as the ratio of the RF field generated by the antenna and the square root of the supplied power

$$\varepsilon_A = \frac{|\mathbf{B_1}|}{\sqrt{P}} \tag{7}$$

$$P = \frac{1}{2}I^2 R_A \tag{8}$$

where the antenna resistance R_A represents losses in the antenna (conductors $R_{\rm cu}$; ferrites $R_{\rm fer}$; and capacitors $R_{\rm cap}$) and

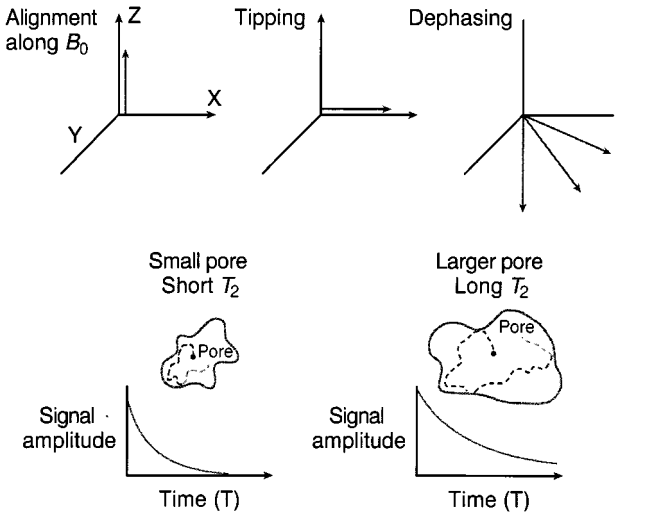

Fig. 4. Spin mechanism of magnetic moments and their relaxation inside a pore of a rock.

the surrounding volume (borehole fluid, R_B; and the formation, R_F), namely

$$R_A = R_{\rm cu} + R_{\rm fer} + R_{\rm cap} + R_B + R_F \tag{9}$$

where all resistances are equivalent series resistances. The inductance L_A and capacitance C_A are given by

$$L_A = L_{\rm fer} + L_{\rm ext} + L_{\rm int} \tag{10}$$

$$C_A = \frac{L_A}{R_A^2 + \omega^2 L_A^2} \approx \frac{1}{\omega^2 L_A}; \quad \text{for } R_A \ll \omega L_A. \tag{11}$$

In (10), $L_{\rm fer}$ is the inductance computed from the magnetic energy stored in the ferrite region while $L_{\rm ext}$ is obtained from the energy stored in the region excluding the ferrite and the conductors. The internal inductance $L_{\rm int}$ is due to the magnetic field penetrating the conductors and is generally negligible. It is given by

$$L_{\rm int} = \frac{R_{\rm cu}}{\omega}. \tag{12}$$

The power loss computation using FEM is quite sensitive to the discretization of antenna conductors. This is because the power loss in an imperfect conductor is caused by the penetrating field. These interior fields decay exponentially along the thickness of the conductor. Consequently, we have to use a very fine mesh along the conductor thickness to accurately represent these fields, and hence to accurately compute the power loss. In several numerical experiments, we found that a discretization with step (Δ) of about one half of the skin depth (δ) and up to a depth of about 5 skin depths gives acceptable accuracy in the power loss computation.

At 2 MHz, the frequency around which the tool is to be operated, the skin depth is 46.73 microns for copper conductors (conductivity, $\sigma = 5.8 \times 10^7$ S/m). This requires the discretization step to be 23 microns along the thickness of the conductor. Along the axial direction, however, we can have large discretization step since axially, for quasi-TEM case, the field varies rather smoothly. Such discretization gives elements with very high aspect ratio that sometimes create numerical

instability. Also, the computation time is enormous because of large number of elements such a discretization creates. We, therefore, use a perturbation technique to evaluate the power loss. This is based on the fact that the power loss can be computed from the knowledge of the tangential magnetic field on the conductors and that these external (to the conductor) fields, in case of quasi-TEM propagation, do not change significantly with the discretization of the conductors.

Consider an infinitely long two-wire transmission line with arbitrary cross section as shown in Fig. 5. The transverse components of the magnetic and electric field can be written as

$$\mathbf{E}_t = \mathbf{e}(x,y)V(z); \quad \mathbf{H}_t = \mathbf{h}(x,y)I(z), \text{ with}$$
$$\int_{C_V} \mathbf{e}\cdot\mathbf{d}\ell = 1, \quad \text{and} \quad \int_{C_I} \mathbf{h}\cdot\mathbf{d}\ell = 1 \tag{13}$$

where the subscript t stands for the transverse components.

For a line with an imperfect conductor, a TEM wave solution is not possible. In general, all the components of the electric and magnetic fields will be present. However, at lower frequency, we can assume the current to be only axial. In other words, we assume that there is no axial component of the magnetic field. The surface current on a conductor is

$$J_{sz} = \hat{\mathbf{z}}\cdot\mathbf{J}_s = \hat{\mathbf{z}}\cdot\hat{\mathbf{n}}\times\mathbf{H}_t = H_\tau. \tag{14}$$

The resistance per unit length of an imperfect conductor with thickness much larger than the skin depth is given by [16]

$$R = \frac{1}{\sigma\delta I^2}\int_{C_1\cup C_2} |H_\tau|^2\, dl. \tag{15}$$

This formula is used to compute the losses in the antenna conductors R_{cu} by first calculating the tangential field around the conductors using an FEM program. The resistances representing losses in the ferrite and the capacitors are computed in the usual way from the respective quality factors, Q_{fer} and Q_{cap} as

$$R_{\mathrm{fer}} = \frac{\omega L_{\mathrm{fer}}}{Q_{\mathrm{fer}}} \tag{16}$$

and

$$R_{\mathrm{cap}} = \frac{1}{\omega C_A Q_{\mathrm{cap}}} \tag{17}$$

while the resistances R_B and R_F are obtained by using the relation

$$R_p = \frac{1}{I^2}\iiint \mathbf{E}\cdot\mathbf{J}^*\, dV_p \tag{18}$$

where $p = B, F$ refer to the regions occupied by the borehole fluid and the formation, respectively.

C. Magnet Design

The magnet is built by stacking several magnet segments along the axial direction as shown in the Fig. 3. The antenna length is generally smaller than the length of the magnet. The additional magnet length provides "prepolarization region" so that the magnetic dipoles of the formation can be polarized while the sensor is moving before an RF pulse can be applied.

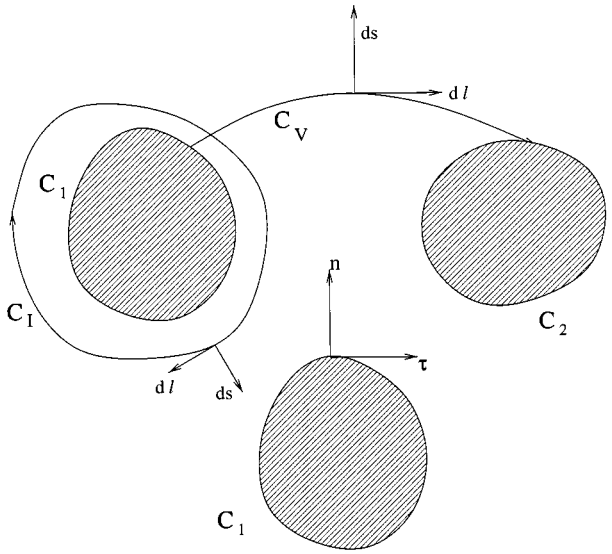

Fig. 5. Cross section of a two-wire line and various integration regions.

The objective of the design is to magnetize each magnet segment in such a way so as to produce a desired field profile in front of the sensor. Since it is highly inefficient to use nonlinear FEM model directly for such a design due to reasons mentioned earlier, we describe here an optimization procedure to improve the numerical efficiency.

The magnetic field generated by the permanent magnet satisfies the equations

$$\begin{cases} \nabla\times\left(\frac{1}{\mu}\mathbf{B_0}\right) = \nabla\times\mathbf{M} \\ \nabla\cdot\mathbf{B_0} = 0 \end{cases} \tag{19}$$

along with appropriate boundary conditions. Here, $\mathbf{M}$ is the net magnetic dipole moment per unit volume. Our objective is to find a suitable excitation $\mathbf{M}$ so that the magnet produces a desired magnetic field profile $\mathbf{B_0}$ in the volume V_1 (see Fig. 3). Our problem, therefore, is to minimize

$$\mathcal{J}(\mathbf{M}) = \int_{V_1} (|\mathbf{B_0}| - B_{\mathrm{RF}})^2\, dv \tag{20}$$

with $\mathbf{M}\in S_M := \{\mathbf{M} = \mathbf{M}_k \text{ in } \Omega_k; \mathbf{M}_k\cdot\hat{\mathbf{z}} = 0\}$. In (20), B_{RF} is the specified field magnitude at the saddle point. In addition to obtaining certain fixed value of $|\mathbf{B_0}|$ at a given location in the formation, we also need to have a saddle point along the Y-direction and uniformity of the field in the axial direction (Z). The zero derivative condition along X is automatically satisfied due to the symmetry of the problem. Combining all these requirements, the objective function becomes

$$\mathcal{J}(\mathbf{M}) = C_1\int_{V_1}(|\mathbf{B_0}| - B_{\mathrm{RF}})^2\, dv + C_2\int_{V_1}\left(\frac{\partial|\mathbf{B_0}|}{\partial y}\right)^2 dv + C_3\int_{V_1}\left(\frac{\partial|\mathbf{B_0}|}{\partial z}\right)^2 dv \tag{21}$$

where the positive constants C_1, C_2, and C_3 are selected to make the three terms equally significant.

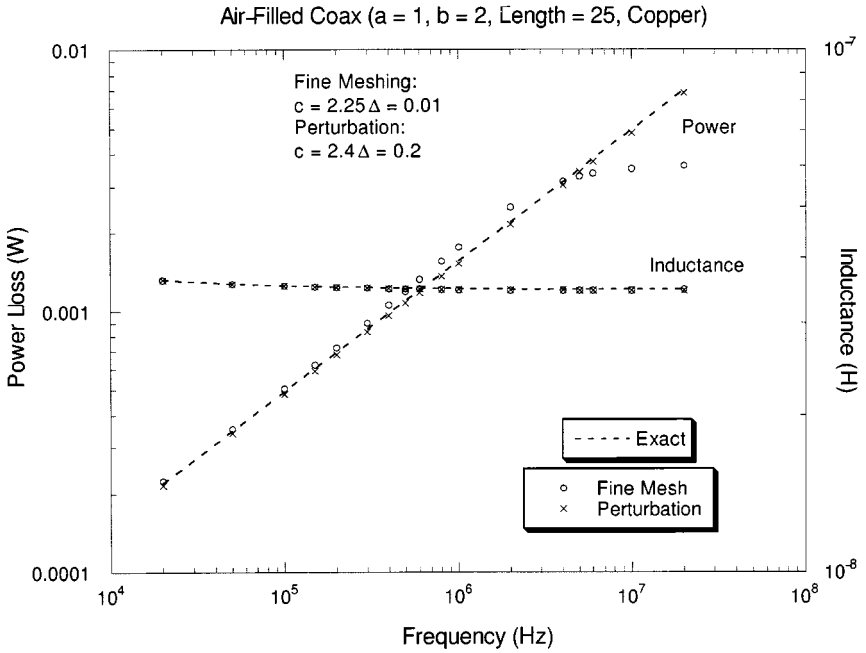

Fig. 6. Power loss and inductance of a coaxial line with the radius: 1) of the inner conductor $= 1.0$ cm and the inner radius; 2) of the outer conductor $= 2.0$ cms. Two discretization steps (Δ) of 0.01 cm and 0.2 cm have been used for the conductor regions. 3) The outer radii of the outer conductor are 2.25 cm for $\Delta = 0.01$ and 2.4 cm for $\Delta = 0.2$. The line is 25 cm long and is made up of copper.

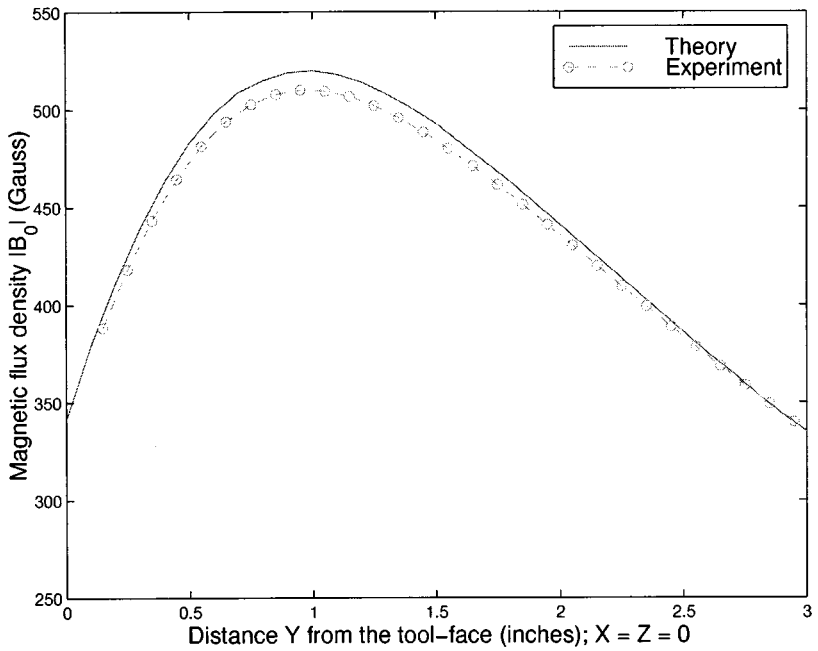

Fig. 7. Measured and computed static magnetic field for NMR magnet.

There are some other constraints as well that we enforce in the actual design. These, for instance, may include the requirement for the field in the volume V_2 to satisfy certain prepolarization constraints to account for the tool motion. Sometimes we also need to avoid large deviation in the magnetization angles of two consecutive magnet pieces for some practical considerations. But to understand our approach of designing the magnet, it is sufficient to consider (21) as the cost function. One of the magnets that we have designed has 228 416 unknowns. Execution of one nonlinear model takes about 30 h of CPU time. A straightforward optimization of (21) requires many iterations; hundreds of iterations are not uncommon. Consequently, the design process becomes exorbitantly time consuming. There is a need to devise efficient strategies to tackle such problems. One such approach is discussed in this section.

We start the design process by assuming an initial magnetization vector $\mathbf{X_0} \in S_M$ and solving the nonlinear FEM problem. Permeabilities of each finite element of the nonlinear materials (ferrite, steel, etc.) are replaced by a single permeability based on the BH curve of the corresponding material and the mag-

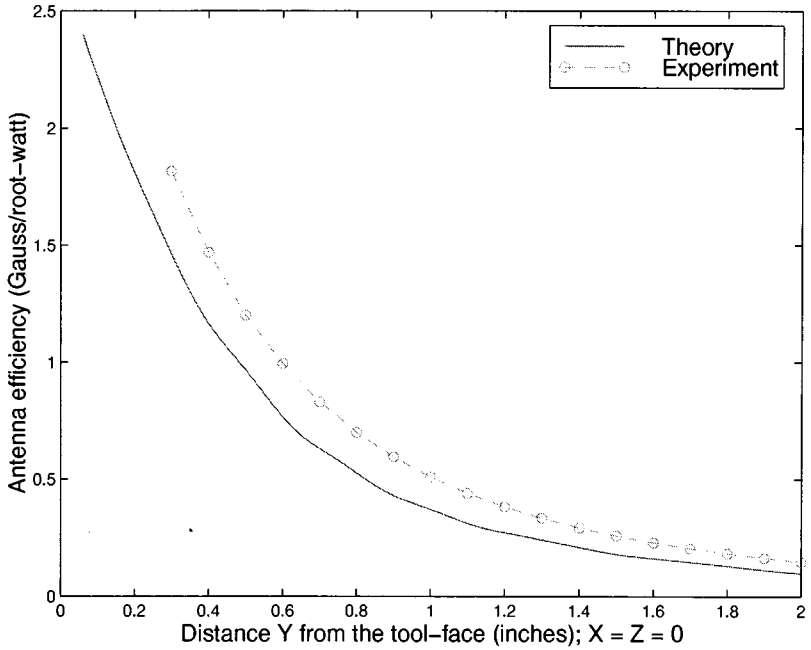

Fig. 8. Measured and computed antenna efficiency ($B_{1x}/\sqrt{P}$); P is the total power loss (copper, ferrite, and capacitor) in the antenna.

netic field computed from the nonlinear modeling. This reduces all the nonlinear magnetic materials with linear inhomogeneous magnetic materials. We then generate a set of basis functions for each magnet segment. That is, magnetic field is computed by magnetizing each magnet segment in two orthogonal directions while keeping the rest of the segments unmagnetized. It is worth mentioning here that a linear model requires about an hour for its solution. Once we have all the basis fields computed, we can obtain the field due to an arbitrary magnetization angle just by superposition of the base fields.

The method of finding the optimal set of magnetization vector $\mathbf{M}$ may be summarized as follows:

$$\begin{cases} \text{Initialize } \mathbf{X_0} \in S_M, \text{ first guess of } \mathbf{X} \\ \text{For } k = 0, 1, \ldots, \text{ do} \\ \quad \mathbf{B_0^k}\text{: solution of the nonlinear forward model} \\ \qquad \text{with excitation } \mathbf{X_k} \\ \quad \begin{cases} \text{Minimize} \\ \quad \mathcal{J}(\mathbf{d_k}) = C_1 \int_{V_1} \left(|\mathbf{B_0^k} + \beta_\mathbf{k}| - B_{\mathrm{RF}}\right)^2 dv \\ \qquad\qquad + C_2 \int_{V_1} \left(\frac{\partial |\mathbf{B_0} + \beta_\mathbf{k}|}{\partial y}\right)^2 dv \\ \qquad\qquad + C_3 \int_{V_1} \left(\frac{\partial |\mathbf{B_0} + \beta_\mathbf{k}|}{\partial z}\right)^2 dv \\ \text{with } \nabla \times \left(\frac{1}{\mu_k}\beta_k\right) = \nabla \times \mathbf{d}_k; \end{cases} \\ \quad \mathbf{X_{k+1}} \leftarrow \mathbf{X_k} + \mathbf{d_k} \\ \text{until } \mathbf{X_k} \text{ converge.} \end{cases}$$

Observe that the field $\beta_\mathbf{k}$ is the correction to the nonlinear field $\mathbf{B_0^k}$ that is added at every iteration of outer loop and that this field $\beta_\mathbf{k}$ can be easily computed by linear combination of the basis field. So while the inner loop takes many more iterations (a few hundred) compared to the outerloop (usually less than ten), the overall computation time is drastically reduced compared with a direct optimization of (21). The only time consuming part is the solution of the nonlinear model in the outerloop. We have used quasi-Newton algorithm for the optimization process, which takes insignificant amount of time (a couple of minutes), when compared with one nonlinear FEM solution for the outerloop (a couple of days). Further details on the magnet design may be found in [17].

III. Results and Discussion

In our design, we use a commercially available three-dimensional FEM software. The design process begins with the optimization of the magnet where we use static magnetic field solver. As mentioned in Section II-C, the optimization process involves solving both the linear and nonlinear static problems. Once we know $\mathbf{B_0}$, we then compute the permeability of the ferrite as a function of position and use that to solve RF problem using linear time-harmonic field solver. We have verified the accuracy of the field computation by solving some canonical problems and comparing them with the analytical solutions. Copper loss computations using (15) have also been verified for a number of cases. Excellent agreement is found between the computed and the exact results. One such result is shown in Fig. 6 where we have plotted power loss and inductance of a coaxial line as a function of frequency for two different discretization steps for the conductor regions. Observe that after about 100 kHz ($\delta = 0.021$ cm), the power loss obtained directly from FEM with fine mesh ($\Delta = 0.01$ cm $\approx \delta/2$) starts deviating from the exact solution since the discretization is no longer adequate, whereas a combination of FEM and perturbation method continues to give good results even with a very coarse mesh size ($\Delta = 0.2$ cm). Inductance calculation, on the other hand, is not influenced by the discretization of the conductors since the internal inductance due to field penetrating the conductors is usually very small (see [12]).

The sensor that we designed has a 30-in-long magnet and a 6-in-long antenna. The magnet was built with 24 segments, each

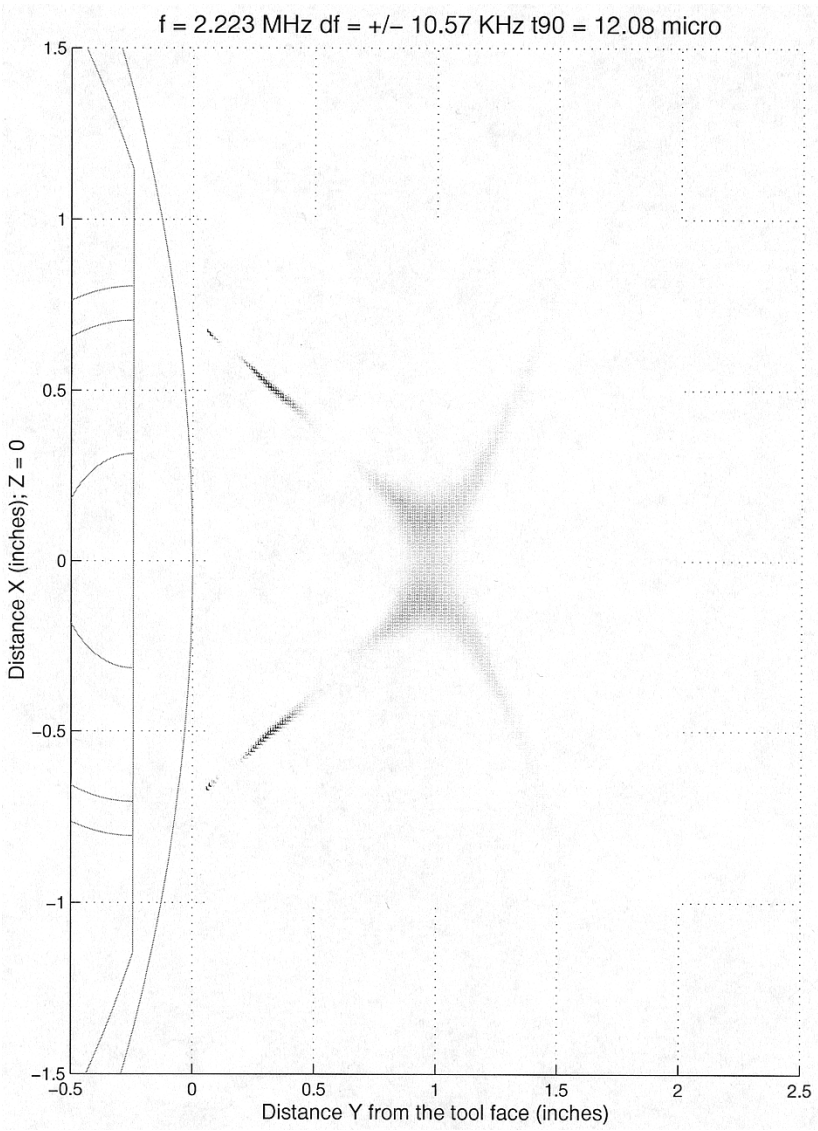

Fig. 9. NMR signal profile in the transverse plane at $Z = 0$; df is the receiver bandwidth; $t90$ is the width of the 90° RF pulse in microseconds. Antenna is 6 in long.

1.25 in in width. The magnitude and direction of magnetization of each magnet segment are adjusted to get the desired field profile, thus giving the dimension of the parameter space as 48. Samarium cobalt has been found to be the best magnet material for borehole applications. It has a residual magnetization greater than one Tesla and a Curie temperature of 820 °C. The residual magnetization of samarium cobalt changes by about 5% between 25 and 175 °C. The sensor is designed to sample a formation region that is about 1.1 in from the face of the tool. The volume V_1 for optimization [see (21) and Fig. 3] is a box $[0, 0.3] \times [1.0, 1.2] \times [-3, 3]$ cubic inches, assuming the origin of the volume to be at the tool face midway along the antenna. The electronic circuitry that drives the antenna and processes the received signal has the operating frequency range of about 1900–2300 kHz. Therefore, in our optimization, we have selected B_{RF} to be 520 Gauss ($\gamma \times 520/2\pi = 2214$ kHz). The second term in (21) ensures a saddle point in the volume V_1 whereas the third term makes field uniform along the axial direction. The first term requiring certain fixed magnitude of $\mathbf{B_0}$ may itself give the best SNR, but the other two terms are required for a variety of reasons including tuning of the antenna and to account for the tool motion.

Figs. 7 and 8 show the comparison of the computed and measured results for the static magnetic field and the antenna efficiency. The results for Fig. 8 are for $\sigma_B = \sigma_F = 0$. We have performed numerous tests with different formation conductivities and have found that the computed and measured results match fairly well. The quality factor of the ferrite was 100, a value supplied by the manufacturer of the ferrite material. For the capacitor we have used 330 as the quality factor. This number was experimentally obtained. The computed antenna efficiency is somewhat lower than the experimental values. We generally take conservative values of the material parameters so that the design exceeds our expectation. It is very difficult to consistently maintain the quality of ferrites and capacitors. So, the discrepancy could be attributed to material properties and some numerical and experimental inaccuracies inherent in any modeling and experiments.

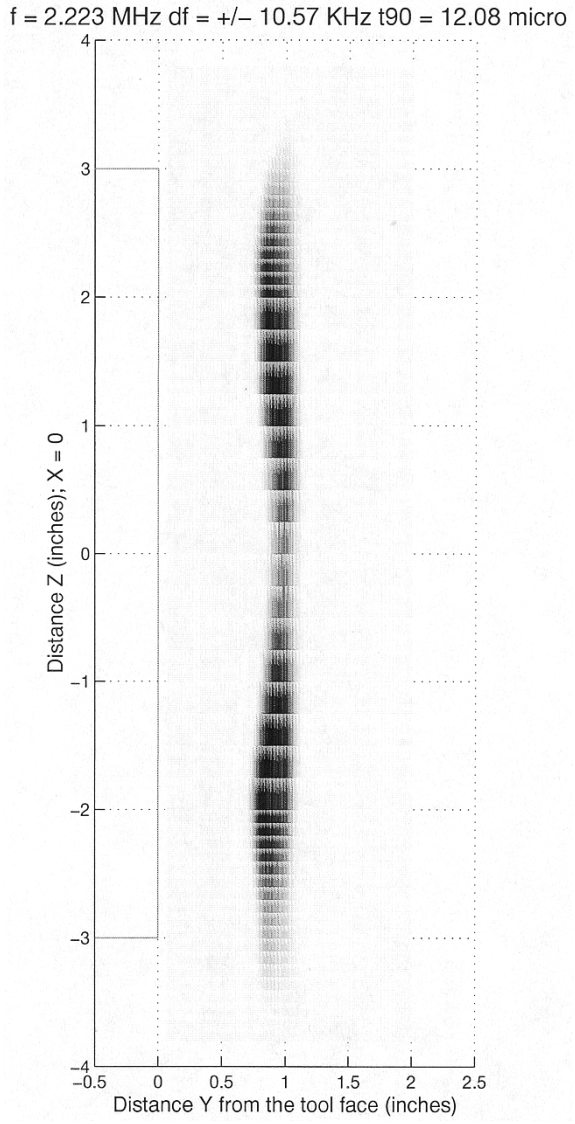

Fig. 10. NMR signal profile in the axial plane at $X = 0; df$ is the receiver bandwidth; $t90$ is the width of the 90° RF pulse in microseconds. Antenna is 6 in long.

We should point out here that we have compared computed and measured field values at other positions as well. But instead of including too many plots, we think it is worthwhile to include a plot on the SNR, something that is after all the main deciding factor in evaluating any design. Furthermore, the computation of SNR takes into account both the RF and static field computations as well as the transfer function of the receiver and spin dynamics.

Figs. 9 and 10 show the signal profile in the transverse and axial plane. Resonant regions are well depicted. The signal levels shown are for RF frequency of 2223 kHz and receiver bandwidth of ± 10.57 kHz (equivalent $|\mathbf{B_0}| = 522 \pm 2.5$ Gauss). These plots provide important information about the performance of the tool. For instance, information such as effective depth of investigation, limitations on the logging speed or, alternatively, the highest T_1 that can be achieved for a given logging speed, and many more can be deduced from these plots. Furthermore, the combination of the gradient-map of $|\mathbf{B_0}|$ and the signal profile can be used to estimate diffusion constant of protons. This parameter is vital, for example, in distinguishing oil and gas.

The SNR is evaluated by assuming a matched filter receiver. Therefore, this number represents the maximum attainable SNR. The SNR computation does not include noise generated by various electronic components and the magnetoacoustic ringing. In practice, therefore, we always get somewhat lower SNR. The computed Larmor frequency of the tool that we designed is 2223 kHz while in experiment the frequency was found to be 2217 kHz. The measured SNR was 2.22 dB lower than the computed value.

IV. Conclusion

In this paper we have presented analysis and design of a complete NMR sensor for oilfield exploration. There are many good electromagnetic computation softwares available these days. A direct use of these softwares may not always be effective. We have to adapt them and augment them with additional numerical techniques for the problem at hand. In particular, in this paper, we have shown how a perturbation technique can be combined with FEM to evaluate power loss in conductors without fine discretization of the conductors and thereby to improve the accuracy and efficiency of the method. We have also presented an optimal control technique which when combined with nonlinear FEM greatly enhances the magnet design process. Finally, we have validated our approach by comparing the measured and computed results for static magnetic field, antenna efficiency, and SNR of the sensor.

References

[1] R. K. Cooper and J. A. Jackson, "Remote (inside-out) NMR: Part I—Remote production of homogeneous magnetic field," *J. Magn. Resonanace*, vol. 41, pp. 400–405, 1980.

[2] L. J. Burnett and J. A. Jackson, "Remote (inside-out) NMR: Part II—Sensitivity of NMR detection for external samples," *J. Magn. Resonance*, vol. 41, pp. 406–410, 1980.

[3] J. A. Jackson, L. J. Burnett, and J. F. Harmon, "Remote (inside-out) NMR: Part III—Detection of nuclear magnetic resonance in a remotely produced region of homogeneous magnetic field," *J. Magn. Resonance*, vol. 41, pp. 411–421, 1980.

[4] H. Clow, W. S. Percival, and P. E. Walters, "Nuclear magnetic logging,", U.S. Patent 4 629 986, Dec. 1986.

[5] S. Strikman, "Nuclear magnetic resonance sensing apparatus and techniques,", U.S. Patent 4 710 713, Dec. 1987.

[6] Z. Taicher, S. Strikman, and M. Shporer, "Nuclear magnetic resonance sensing apparatus and techniques,", Jan. 1988.

[7] R. L. Kleinberg, D. D. Griffin, M. Fukuhara, A. Sezginer, and W. C. Chew, "Borehole measurement of nmr characteristics of earth formations,", Oct. 1991.

[8] R. L. Kleinberg, A. Sezginer, D. D. Griffin, and M. Fukuhara, "Novel NMR apparatus for investigating an external sample," *J. Magn. Resonance*, vol. 97, pp. 466–485, 1992.

[9] A. Sezginer, D. D. Griffin, R. L. Kleinberg, M. Fukuhara, and D. G. Dudley, "RF sensor of a novel NMR apparatus," *J. Electromagn. Waves Applicat.*, vol. 7, pp. 13–30, 1993.

[10] T. C. Farrar and E. D. Becker, *Pulse and Fourier Transform NMR*. New York: Academic, 1971.

[11] Z. H. Cho, H. S. Kim, H. B. Song, and J. Cumming, "Fourier transform nuclear magnetic resonance tomographic imaging," *Proc. IEEE*, vol. 70, pp. 1152–1173, 1982.

[12] W. S. Hinshaw and A. H. Lent, "An introduction to NMR imaging: From the Bloch equation to the imaging equation," *Proc. IEEE*, vol. 71, pp. 338–350, 1983.

[13] R. L. Kleinberg, W. E. Kenyon, and P. P. Mitra, "Mechanism of NMR relaxation of fluids in rock," *J. Magn. Resonance*, vol. 108, pp. 206–214, 1994.
[14] H. Y. Carr and E. M. Purcell, "Effects of diffusion on free precession in nuclear magnetic resonance experiments," *Phys. Rev.*, vol. 94, pp. 630–638, 1954.
[15] S. Meiboom and D. Gill, "Modified spin-echo method for measuring nuclear relaxation times," *Rev. Sci. Instrum.*, vol. 29, pp. 688–691, 1958.
[16] R. Plonsey and R. E. Collin, *Principles and Applications of Electromagnetic Fields*. New York: McGraw-Hill, 1973, p. 368.
[17] B. Luong, J. C. Goswami, A. Sezginer, and D. Davies, "An optimal control technique for magnet design in inside-out NMR," IEEE Trans. Magn., to be published.

Jaideva C. Goswami (S'86–M'95–SM'99) was born in 1964 in Khutauna, India. He received the Ph.D. degree in electrical engineering from Texas A&M University, College Station, in 1995.

He was in the faculty of Electrical and Computer Engineering Department of Regional Engineering College, Surat, India, in 1987. From 1989 to 1991, he worked as a Research Engineer at the Advanced Center for Electronic Systems, Indian Institute of Technology, Kanpur. After spending one year at the University of Illinois at Urbana-Champaign as a Postdoctoral Research Associate, he joined Schlumberger Well Services, Sugar Land, TX, in 1996, where he is currently a Senior Engineer. Besides publishing a number of papers in journals and conference proceedings, he has contributed three book chapters and is a coauthor of *Fundamentals of Wavelets: Theory, Algorithms and Applications* (New York: Wiley, 1999). His research interests include computational electromagnetics, wireless communication, remote sensing, nuclear magnetic resonance, and signal processing.

Dr. Goswami is a member of Society of Professional Well-Log Analysts.

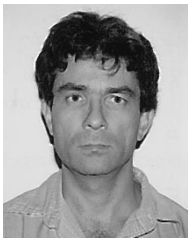

Apo Sezginer (SM'91) was born in Istanbul, Turkey, in 1958. He received the Ph.D. degree in electrical engineering from the Massachusetts Institute of Technology, Cambridge, in 1985.

From 1985 to 1996, he was with Schlumberger-Doll Research and, since 1997, he has been with Schlumberger Sugar Land Product Center. His research interest include mathematical modeling of electromagnetic fields and waves, mathematical modeling of nuclear magnetic resonance apparatus with inhomogeneous fields, signal processing, and optimization. He contributed to the development of the hardware and processing of the combinable magnetic resonance logging tool. He is the inventor or coinventor of 12 U.S. patents.

Bruno Luong was born in Saigon (now Ho Chi Minh City), Vietnam, on October 6, 1966. He received the Ph.D. degree in applied mathematics from the University Josheph Fourier, Grenoble, France, in 1995.

From 1995 to 1996, he was with the University of Minnesota, Minneapolis, as a Postdoctoral Research Associate. He joined Schlumberger Oilfield Services, Sugar Land, TX, in March 1997 where he has been involved in modeling, analysis, development, and design of well-logging tools. His research activities includes computational fluid dynamics, control problem, data assimilation, electromagnetic theory, and inverse problems.

Dr. Luong is a member of American Mathematical Society.